Mixing of a continuous flow of two fluids due to unsteady flow

R. A. Truesdell,[1] P. V. Vorobieff,[1] L. A. Sklar,[2] and A. A. Mammoli[1]
[1]*Department of Mechanical Engineering, The University of New Mexico, Albuquerque, New Mexico 87131, USA*
[2]*Department of Pathology, University of New Mexico Health Sciences Center, Albuquerque, New Mexico 87131, USA*
(Received 12 June 2002; revised manuscript received 9 December 2002; published 13 June 2003)

In many low-Reynolds number mixing applications, the absence of turbulence makes it difficult to achieve proper mixing of two fluids. In this paper, flow visualization is used to obtain quantitative measurements of mixing that occurs when combining two pulsatile fluid streams at a Y-connection. Mixing results from the interface distortion created by the pulsatile flow. This is generated by combining the action a peristaltic pump, which provides the mean flow, with the action of two pinch valves, one on each arm of the Y-connection, to generate strong pulsations. The action of the pinch valves is be controlled via pulse generators. Apparently chaotic conditions were realized in the confluence region, superimposed with the mean flow. The valve action was optimized to maximize mixing, the latter quantified via image analysis. This work demonstrates a low cost, efficient mixing device for low-Reynolds number conditions, which is therefore suitable for miniaturization.

DOI: 10.1103/PhysRevE.67.066304 PACS number(s): 47.15.−x, 47.52.+j, 47.60.+i

I. INTRODUCTION

Problems involving mixing of two fluids or gases are ubiquitous and span the entire range of scales that can be considered in hydrodynamics—from astrophysics to nanomachinery. Quality of mixing is essential for many applications, especially those involving chemical reactions. For these applications, mixing on the larger scales is easier to achieve, in a sense. Large scales are typically associated with large-Reynolds numbers Re, and the latter with turbulence, which greatly enhances mixing processes. However, applications also exist where the characteristic scales and velocities are too low for transition to turbulence, but diffusive mixing usually associated with laminar flow is insufficient. One example of such an application is drug discovery through high throughput flow cytometry [1], which requires the capacity to mix a large number of very small fluid samples at a high rate. As a consequence of the sample size, it is desirable to minimize the dimensions of the flow, inevitably leading to a laminar flow regime. In a recently developed microfluidic system currently under investigation for use in drug discovery [2], two reagent streams are introduced into a single channel via a Y-connection, and the combined stream is analyzed by the flow cytometer further downstream. Ideally, the reagents in the merged stream are thoroughly mixed by the time the sample reaches the cytometer.

Molecular diffusion is the fundamental mechanism of mixing. Mixing is enhanced by the reduction of the distance that a fluid molecule must travel to encounter fluid of a different phase, the diffusion distance. This is generally achieved by stretching and folding of interfaces. Sadly, while stretching and folding occurs naturally in turbulent flows, it is difficult to achieve in laminar flow conditions, that is, at low to moderate Reynolds numbers.

Stretching and folding of interfaces at low Re can be generated by suitable positioning of the interface within a contained flow—a driven cavity [3–5]. It is well-known that chaotic flow generated by aperiodic motion of the cavity walls leads to efficient and complete mixing. Periodic motion of the walls can also generate chaos, but mixing in such cases is less efficient and some regions may remain unmixed [6]. Finally, steady motion does not generate chaotic flows. The basic mechanisms of chaotic mixing in a cavity are described qualitatively by Ottino [7], and in more detail by Ottino *et al.* [4]. The relative merits of the computational and experimental approaches in the study of mixing are addressed by Swanson and Ottino [8], Souvaliotis *et al.* [9], and Jana *et al.* [10], where it is concluded that, while numerical simulation can provide information on the flow field at a level of detail hard to obtain experimentally, its application to the simulation of mixing is limited by the difficulty in describing the evolution of the interface. In general, a combination of numerical, mathematical, and experimental tools is necessary for a complete study. On the other hand, Leong and Ottino [11] suggest that valuable insight into the complex behavior of seemingly simple flows can be gained solely by experimentation.

Sample delivery systems involving pipe flows of liquid samples separated by gas bubbles are important for many applications, including cytometry. Usually, the length of individual samples compared to the cross-sectional dimension of the mixing device is such that the flow may be considered continuous, rather than contained. However, the cross-section of the conduit (normal to the direction of the mean flow) may be viewed as a contained region, and hence the methodology used to enhance mixing in driven cavities can be applied. As an example, Strook *et al.* [12] use ridges placed on one of the conduit walls to induce periodic motion in the plane normal to the flow direction, thus achieving chaotic mixing. In a similar fashion, Khakhar *et al.* [13] describe the action of the partitioned-pipe mixer, which consists of a sequence of semicircular ducts where the walls rotate coaxially relative to fixed orthogonal plates. A full mathematical description of the flow is used to obtain Poincarè sections, describing some features of the chaotic nature of the flow. Other parameters such as residence time, mixing strength, and stretching efficiency are given to fully characterize the effectiveness of mixing. This flow is similar in nature to the flow found in certain commercially available static inline mixers.

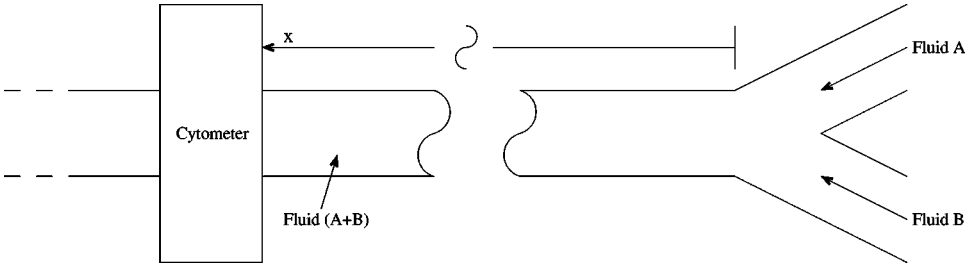

FIG. 1. Schematic of the mixing flow. Fluids *A* and *B* are introduced at each arm of a Y-connection, and the resulting combined stream is measured downstream with a cytometer.

In many chemical and biological applications, the fluid contains suspended rigid particles or cells, which may be trapped by obstacles in the flow such as partitions or serrated walls. In flow cytometry, any fluid retention from a sample will transfer to the following sample, thus compromising the validity of the cytometer measurement. A mixing device characterized by smooth walls and the absence of obstructions should minimize such undesirable effects. The simulation of a converging-diverging channel [14], where the radius of the flow is sinusoidal, shows that mixing in the plane parallel to the flow is possible, and that at high enough Re, chaos ensues. Mixing is also possible in a channel where the deformation of one of the walls is described by a small-amplitude traveling wave [15].

The necessity for better understanding of the low-Re mixing reagent flow through a Y-connection [2] serves as one of the motivations of this paper. Besides quantification of the mixing process, our goal is to enhance mixing by conditioning the pulsing flow of the reagent streams. However, the physical phenomena we observe in the flow at the Y-connection and downstream of it appear to have more general implications. Flow pulsation can superimpose a disordered component upon the laminar mean flow, resulting in greatly enhanced mixing and apparently chaotic behavior of the system.

It is noteworthy that the geometry of the Y-connection apparatus is strikingly similar to what is commonly found in blood vessels. In addition, similar pulsatile flow conditions arise in both cases. In several studies performed by Taylor and co-workers [16–18], the application of finite element analysis (FEA) to model blood flow in large blood vessels is described. Of particular relevance to this study is the finding that recirculation regions arise in the vicinity of bifurcations as a result of the pulsatile nature of the flow. Their pathological relevance is due to the correlation of such recirculation zones with accumulation of plaques, leading to adverse health effects. For the purposes of the present study, recirculation zones may be viewed as areas of potential mixing enhancement. A study [19] using simplified one-dimensional analysis reaches similar conclusions. In addition, experimental evidence of flow separation inside a model carotid bifurcation is presented. However, the conditions that give rise to these recirculation zones are not present in this investigation. In both the FEA studies and the numerical-experimental work, recirculation appears to be caused by inertial effects, and indeed the Reynolds number reported is ≈ 4000, on the threshold of turbulence. In contrast, the Reynolds numbers typical of the flows considered in the present study do not exceed one. Thus, the mechanisms reported here are expected to be of an entirely different nature.

II. EXPERIMENTAL APPARATUS

The schematic of the flow of interest in this work is presented in Fig. 1. Fluid *A* and fluid *B* are introduced at two joining branches of the Y-connection. Both flows are driven by an upstream peristaltic pump, which introduces a degree of unsteadiness in the flow. A certain amount of mixing has been observed in a similar setup previously [20]. This is thought to be due to stretching and folding of the wavy interface between the two fluids that results from the peristaltic-pumping action. The verification of this theory by flow visualization was the original motivation of the present study.

Visualization of flow in the apparatus used in the experiment described by Jackson *et al.* [20] would be difficult because of optical distortion caused by a mismatch in the refractive index of the mixer and the working fluid. Difficulties are compounded by the small dimensions of the apparatus. For this reason, a scaled-up model was built. For a continuous flow, two-dimensionless parameters are important: the Reynolds number ($\mathrm{Re}=ud/\nu$, where u is a characteristic flow velocity, d is a characteristic dimension, and ν is the kinematic viscosity), which describes the ratio between inertial and viscous forces and the Peclet number ($\mathrm{Pe}=ud/\alpha$, where α is the diffusivity), which describes the ratio of mass transfer by convection to that by diffusion.

A typical setup used with the flow cytometer [20] involves tubing of diameter 2.5×10^{-4} m and a total flow rate of 3.333×10^{-9} $\mathrm{m^3\ s^{-1}}$ (200 μl per min) corresponding to a velocity at each inlet of $0.033\,95$ $\mathrm{m\,s^{-1}}$. With water as the working fluid ($\nu=1.14\times10^{-6}$ $\mathrm{m^2\ s^{-1}}$), the Reynolds number at the outlet of the Y-connection is ≈ 15, well within the laminar flow regime. To simplify the experiment, the limit of no diffusion ($\mathrm{Pe}\gg 1$) and low-Reynolds number ($\mathrm{Re}\ll 1$) is investigated here. This represents the worst-case scenario, and the presence of diffusion can only be beneficial to mixing.

The diameter of the tubing in the scaled-up model is $0.003\,175$ m. Using a 1536×1024 pixel camera with a Sigma 105-mm macrolens and a series of closeup filters to reduce the focal length, it was possible to obtain sufficiently detailed digital images of the flow, with ≈ 250 pixels per diameter length. The image thus contains a section of tube of ≈ 6 diameter lengths. With a flow rate of 42×10^{-10} $\mathrm{m^3\ s^{-1}}$, the Re for the scaled-up model is ≈ 0.31.

Refractive index matching between the mixer model and the fluid is required to allow undistorted imaging of the flow inside the model. The model consists of a Y-connection,

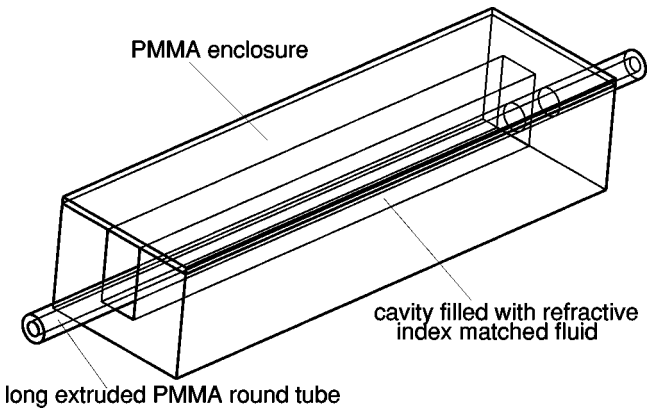

FIG. 2. Schematic of viewing apparatus.

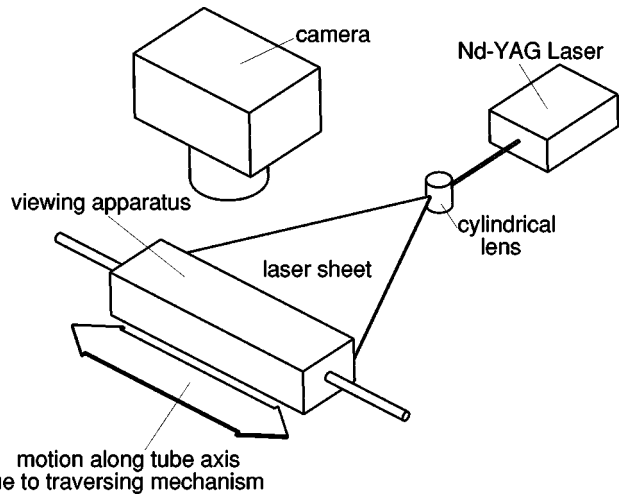

FIG. 3. Schematic of laser-camera-traverse setup.

followed by a long straight tube. The diameter of the arms of the Y-connection and of the long tube are equal. The Y-section is machined from a small block of poly(methyl methacrylate) (PMMA) (refractive index 1.488). Because drilling a long ($\approx$500 diameter lengths) circular channel is impractical, an extruded PMMA tube is placed in a channel milled in a long rectangular PMMA block, as shown schematically in Fig. 2. The gap between the tube and the block is filled with refractive index matched fluid and a thin PMMA sheet is glued to the top of the block to contain the fluid.

A solution of zinc chloride ($ZnCl_2$) and deionized water is used as the working fluid. The refractive index of the solution can be adjusted by changing the amount of $ZnCl_2$ per unit mass of water. A mass ratio of 1.97 parts $ZnCl_2$ to 1 part water results in the correct refractive index, measured using a Mettler-Toledo DR-50 refractometer at 22°C. The rheological properties of the fluid were characterized using a Stresstech rheometer. The fluid is Newtonian, with a viscosity of $\approx$0.02 Pa s at 22°C.

Because everything used in the apparatus including the working fluid has the same refractive index, light travels practically undeflected within any cross section. Cross sections of interest are illuminated by a $<1\times10^{-4}$-m-thick pulsed light sheet obtained by passing a laser beam through a cylindrical and a spherical lens. The laser beam is generated by a New Wave Research Gemini PIV Nd:YAG (Yttrium aluminum garnet) laser, with a pulse duration of 3–5 ns and power of about 20 mJ per pulse. The camera (Kodak Megaplus 1.6i) focused on the laser sheet is mounted above the viewing apparatus, as shown in Fig. 3.

The camera and laser are stationary while the viewing apparatus is mounted on a traversing mechanism, allowing certain features of the flow to be followed if so required. The traversing mechanism is a computer controlled belt driven system. The servo motor is connected to a planetary inline gearhead with a 25:1 ratio. The system has a unidirectional repeatability of $\pm$0.004 mm, an accuracy range of 0.020 mm–0.162 mm, and a backlash range of 0.02 mm–0.04 mm. These specifications are more than adequate for the purpose of this work.

A Gilson Minipuls 3 peristaltic pump with ten rollers drives the fluids. The interface distortion produced by the peristaltic-pumping action is thought to be responsible for the observed mixing of the incoming streams. The amplitude of the interface distortion can be controlled by changing the phase between pulsations in the incoming flows, which in turn is a function of the difference in the lengths of the tubes between the pump head and the mixer inlet. Equal lengths, corresponding to in-phase flow, do not produce interface distortion, while a difference in length equal to half the distance between adjacent rollers maximizes interface distortion.

Increased interface distortion can be obtained by interrupting the flow of either incoming stream by means of pinch valves. Two Neptune Research pinch valves are mounted just upstream of each branch of the Y-connection. They are powered by a 12-V power supply and controlled by two pulse generators. The period and pulse width of one valve are controlled by a master pulse generator. The second valve is controlled by a slave pulse generator, triggered by the first pulse generator with a controlled delay. The period and pulse width of the slave pulse can be controlled independently, however, both are set to the same value as the master pulse to maintain an equal flow rate for both streams. Both pinch valves are normally open. An oscilloscope is used to monitor the valve operation.

One of the streams is seeded with small ($\approx$0.2 μm) titanium dioxide (TiO_2) particles. These particles are very efficient Mie scatterers. Their density is higher than that of the working fluid, but they are sufficiently small to follow the flow without any noticeable settling on the time scale of the experiment. Illumination of the flow by the laser results in a ''light'' stream (seeded) and a ''dark'' stream (unseeded). The tracer amount used is small enough that there is no appreciable change in the density of the fluid. The mixture is $\approx$1 part TiO_2 per 100 000 parts of the $ZnCl_2$ and water solution. The laser pulses are triggered by the camera shutter. Only one laser pulse per image is used. The digital images are acquired via a Bitflow Roadrunner board, and stored on disk for subsequent postprocessing. The average pixel intensities associated with the light and dark streams are subsequently employed to calibrate the images in terms of concentration of the light stream material. The average intensity of dark pixels corresponds to 0% concentration, the correspond-

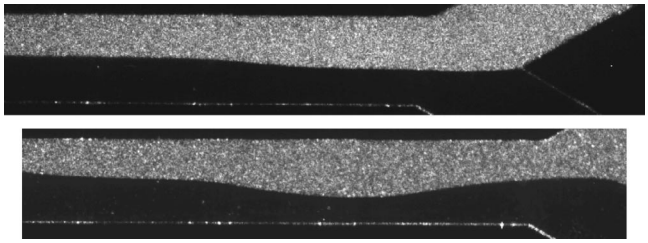

FIG. 4. Interfaces generated by slightly out of phase flow (top) and fully out of phase flow (bottom). Note the difference in amplitude of the interface wave.

ing light intensity is 100%. The intensity-concentration mapping is effectively linear because the light sheet illuminates a thin section of the flow, and the particle-seeding density is low.

III. EXPERIMENTAL RESULTS

A. Peristaltic action

The first batch of experiments visualized the effects of the peristaltic action on the flow patterns at and after the Y-connection. Both incoming streams are driven by the same peristaltic pump. In Fig. 4, interfaces produced by pulsation are shown slightly out of phase (top) and 180° out of phase (bottom). The phase delay was produced by variation of the length of one of the tubes connecting the peristaltic pump to the apparatus.

The formation of a wavy interface eventually leads to folding due to the flow profile. The traversing mechanism was used to follow an individual wave along the tube. Figure 5 shows the formation of a fold. The formation of folds coincides with interface stretching, which promotes diffusion due to the larger interface area. Because of the parabolic mean velocity profile, waves with larger amplitude (out of phase flow) produce faster and more extensive folding. This difference is highlighted in Fig. 6.

At about 82 diameter lengths downstream from the Y-connection, there is only one long fold for the slightly out of phase flow. For the fully out of phase flow there is evidence of two folds at about 62 diameter lengths. Further down the viewing apparatus, at 162 diameter lengths, there is evidence of many folds and the center of the tube is beginning to appear mixed. Clearly, some mixing at the center of the stream is obtained, essentially with no cost, simply due to the peristaltic-pumping action. However, this experiment shows that, if this effect is to be exploited fully, the pulsation of the streams should be 180° out of phase.

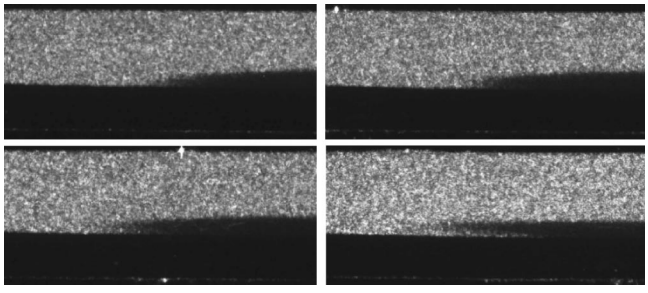

FIG. 5. Picture sequence showing the first fold occurring after the Y-connection for slightly out of phase flow. The picture order is as follows: top left, top right, bottom left, and bottom right.

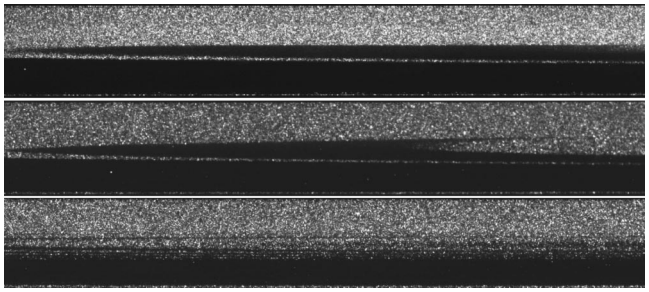

FIG. 6. Folds at 82 diameter lengths downstream from the Y-connection for slightly out of phase flow (top), at 62 diameter lengths for out of phase flow (center), and at 162 diameter lengths for out of phase flow (bottom).

B. Controlled pinch-valve action

The amplitude of the waves generated by the pulsed flow of the input fluids is directly related to the maximum amount of mixing that can occur, since folding and interface stretching can only take place in the volume of fluid contained between the wave crests and troughs. It is interesting to note that a lower quality peristaltic pump is likely to perform better than the ten-roller pump used in this study. Increasing the diameter of the tubing that runs through the pump head results in increased pulsation amplitude. However, the pump speed must be adjusted to compensate for the increased pumping volume, thus producing longer waves, which is detrimental to mixing. In general, reliance on the type of pump and tubing to encourage mixing is probably undesirable.

To better control and enhance the mixing effect provided by the pulsed flow inherent in peristaltic-pumping action, two pinch valves are introduced just prior to each branch of the Y-connection. The pinch valves are similar to the peristaltic action in that they compress the tube just as the peristaltic pump does. The effect is twofold. First, during compression of the tube, a certain amount of positive pumping action is created, while negative pumping action is created upon release. Second, the mean flow of the pinched stream is interrupted for the duration of the valve actuation.

In contrast to the peristaltic-pump action, which is primarily intended to provide a mean flow rate, the action of the pinch valves can be controlled independently. The parameters that can be controlled are the pulse width (the amount of time that the valve is closed), the period (time between pulses), and the delay between the pulses for each incoming stream. As with the peristaltic-pumping action, in-phase pulses in theory would not produce any interface distortion. Three sets of experiments were performed. The three parameters above are nondimensionalized by the time required for a particle at the center of the flow to move 1 diameter length. For these sets of experiments that time is 2.837 s. The first set of experiments is done using a period of ≈ 0.493, the second set using a period of ≈ 0.282, and the third set using a period of ≈ 0.141. Within each of these sets the pulse width and delay are altered. Table I lists a subset of representative

TABLE I. Nondimensionalized pinch valve parameters for different experiments.

Experiment number	Period	Pulse width	Delay
Experiment 1	0.493	0.169	0.187
Experiment 2	0.493	0.044	0.021
Experiment 3	0.282	0.139	0.134
Experiment 4	0.282	0.037	0.035
Experiment 5	0.141	0.070	0.067
Experiment 6	0.141	0.018	0.018

experiments performed and the relative nondimensional parameters.

The steady-state interface configuration in the vicinity of the Y-connection with a period of 0.493, and variations of the pulse width and delay (experiments 1 and 2), is shown in Fig. 7. It appears that mixing is enhanced by a reduction of the pulse width and delay. With the larger pulse width, the interface does not span the entire width of the tube. The situation is improved by reducing the pulse width and the delay.

Reduction of the period further improves mixing. The trend observed in experiments 1 and 2, namely, that a reduction of the pulse width promotes mixing, is evident throughout the experiments, as can be observed in Fig. 8.

In general, mixing improves with a reduction in period, pulse width, and delay. However, clearly a zero delay would not produce a distorted interface, so an optimum value must exist. Also note the qualitative differences between the various experiments: for example, the mixing in experiment 4 is very good, but there remain some small unmixed islands. These disappear in experiment 6, which appears to generate complete mixing.

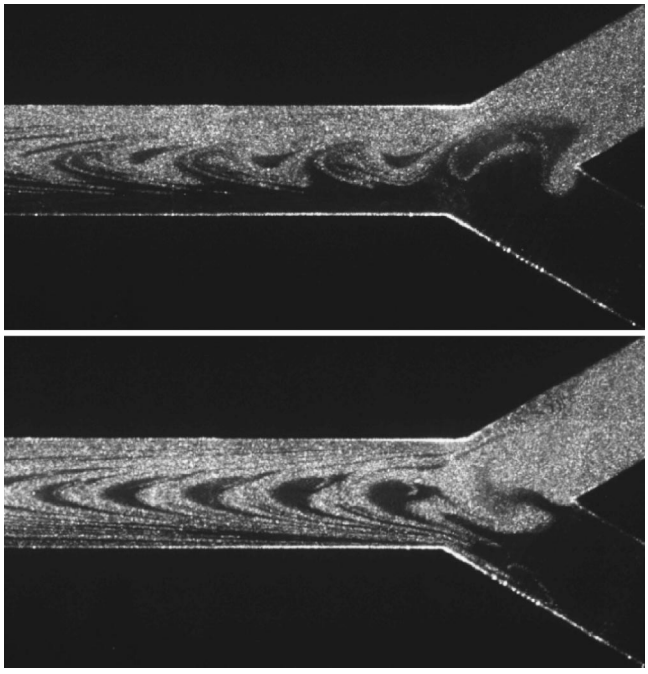

FIG. 7. Pinch-valve experiments 1 (top) and 2 (bottom). Refer to Table I for timing parameters.

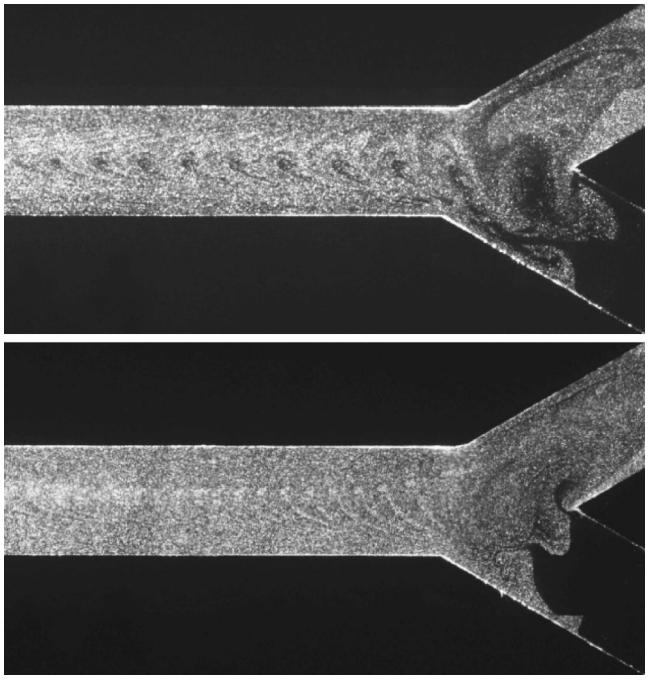

FIG. 8. Pinch valves on: experiment 4 (top), experiment 6 (bottom). Note the marked improvement in mixing that results from simultaneous reduction of the period, pulse width, and delay.

Although the flow retains some periodicity, it appears that a small region of chaotic flow exists at the intersection of the three tubes, superimposed on a mean flow. The relative amount of time that a fluid volume spends in this apparently chaotic region determines the quality of mixing.

The nature of the flow in the intersection region is best visualized by inspection of the transient flow following the onset of the pinch-valve action, shown in Fig. 9 for experiment 5. The interface appears to move from one arm of the Y-connection to the other, and in the process folds over itself, eventually creating striations that are convected downstream by the mean flow. The dominant interface distortion mechanism appears to be the pulsation created by the rapid closure of the pinch valve, rather than the interruption of the flow. There are two possible routes for the fluid transported by the velocity pulsation due to valve shutoff: towards the base of the Y-connection or into the other branch. The latter path promotes further interface stretching and folding. Flow from one branch of the Y-connection into the other is favored if a valve closure in one branch is preceded by a release in the other arm, explaining the improvement of mixing resulting from a reduction in the delay duration. It is noteworthy that, although the flow is driven by periodic action, the visualized tracer pattern at Y-connection never repeats exactly. This is an indication that the flow indeed may be chaotic.

Additional evidence supporting the existence of a chaotic region can be extracted from the analysis of the stationary (i.e., no mean flow) operation of the pinch valves, Fig. 10. The complex patterns formed by the tracer indicate stretching and folding of the mixing interface, eventually leading to a rather well-mixed flow.

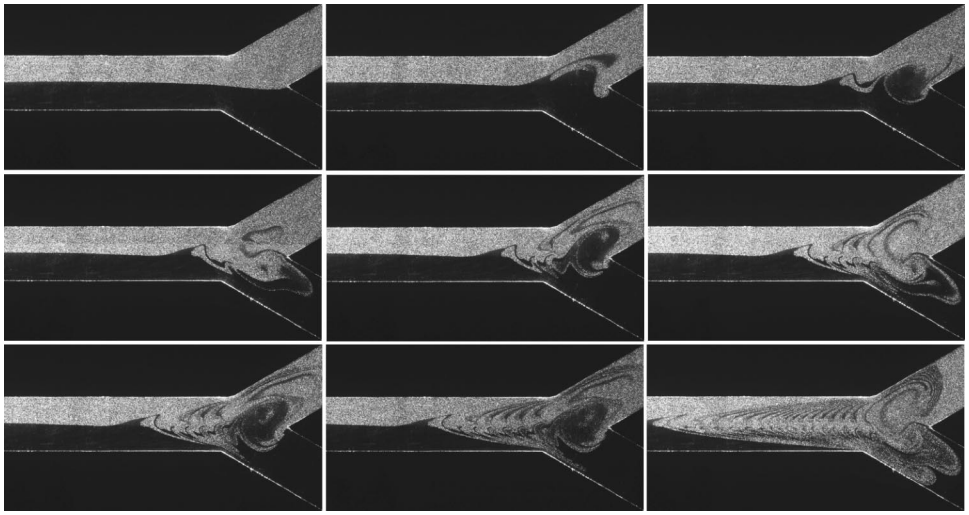

FIG. 9. Transient flow upon startup of the mixer for the parameters of experiment 5. Nondimensionalized times are 0.0, 0.110, 0.242, 0.352, 0.451, 0.688, 0.787, 1.063, 2.528.

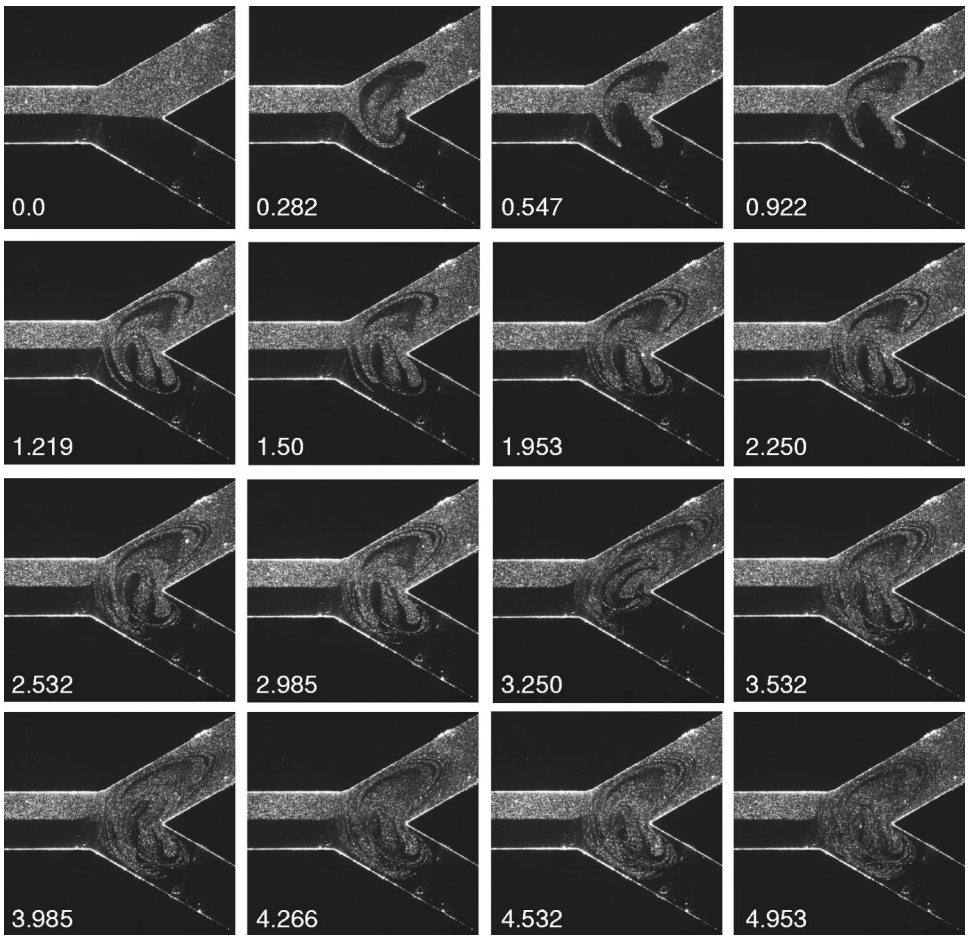

FIG. 10. Startup of the pinch valves with no mean flow for the parameters of experiment 5. Nondimensionalized times are 0.0, 0.282, 0.547, 0.922, 1.219, 1.500, 1.953, 2.250, 2.532, 2.985, 3.250, 3.532, 3.985, 4.266, 4.532, 4.953.

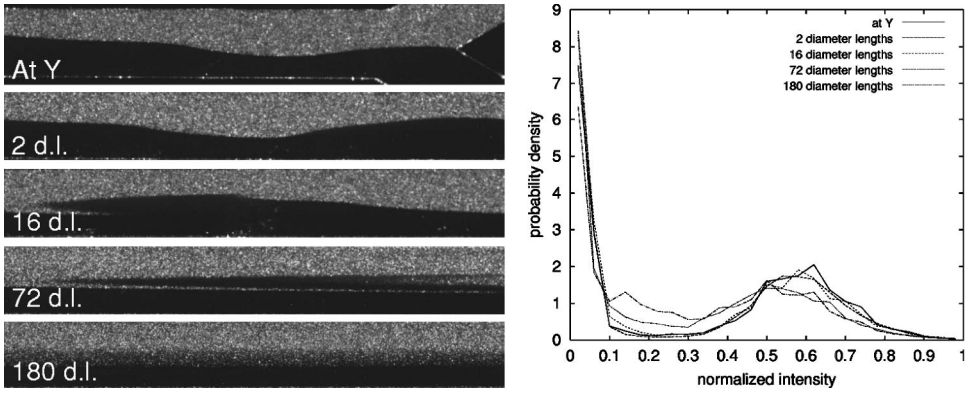

FIG. 11. Histogram plots of peristaltic-pump flow with accompanying pictures at different diameter lengths.

IV. ANALYSIS

Rigorous optimization of the pinch-valve actuation parameters requires a quantitative measure of mixing. The information at hand suggests that image analysis should be used for this purpose, although other more direct means of quantification (such as cytometry) should also be considered.

The goal of the image analysis is to facilitate quantitative measurements of mixing in the flow by recovering the instantaneous concentration fields. First, the images are processed with a filter sensitive to gradient and structure size (''dust and scratch'' filter). This filter removes small-scale ($\sim 5\ \mu$m) intensity fluctuations due to slight nonuniformities in the tracer seeding. The size of the images is then reduced by a factor of 3, effectively smoothing the image further by antialiased downsampling. The lighting intensity varied from experiment to experiment, and it was therefore necessary to normalize the overall intensity of each image. The grayscale values of all pixels in the image were binned. The lowest and highest intensity bins that contained a set number of pixels were chosen as the minimum and maximum range limits. Intermediate grayscale values were scaled accordingly. Thus, occasional bright spots (for example, reflections from a bubble) were eliminated. This normalization is motivated by the interpretation of pixel intensity as local concentration of the material of the light stream.

Histograms of grayscale values from the filtered images represent the probability density of finding a pixel at a given intensity. These are scaled so that the total probability is 1. Images for fully out of phase peristaltic flow at different distances downstream of the Y-connection, accompanied by the respective histograms, are shown in Fig. 11. The histogram for the initial unmixed configuration (at the Y-connection) shows a population of light pixels and a somewhat more diffuse population of dark pixels. These features persist further downstream, however, an intermediate gray population between the two emerges. This is fully consistent with the qualitative information contained in the images.

Images and accompanying histograms for experiment 2 are shown in Fig. 12. The qualitative difference that can be discerned by inspection of the images is reflected in the histograms. The dark population (the islands) is reflected in the lower peak in the histogram for $x/d=0$, accompanied by a diffuse light peak. Because of the stretching action of the flow, the sharpness of the black peak is reduced as the flow proceeds downstream. Finally, the histogram for experiment 4, shown in Fig. 13 displays an almost indistinguishable black peak, which soon disappears. The histograms at $x/d=154$ and $x/d=264$ show an almost normal distribution, indicating complete mixing.

The correspondence in the qualitative features of the images and the corresponding histograms suggest that a ''mixing parameter'' M_1 could be obtained from the histograms. The first moment of the histogram [defined by the probability density $p(x)$, where x is the grayscale value] about its centroid is defined as

$$M_1=\int_0^1 rp(x)dx, \tag{1}$$

where $r=|x-\overline{x}|$ and the centroid $\overline{x}$ is given by

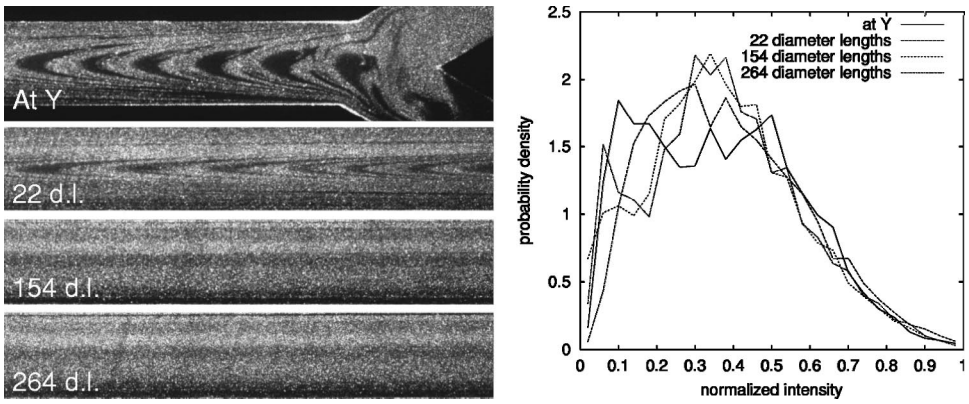

FIG. 12. Histogram plots of experiment 2 with accompanying pictures at different diameter lengths.

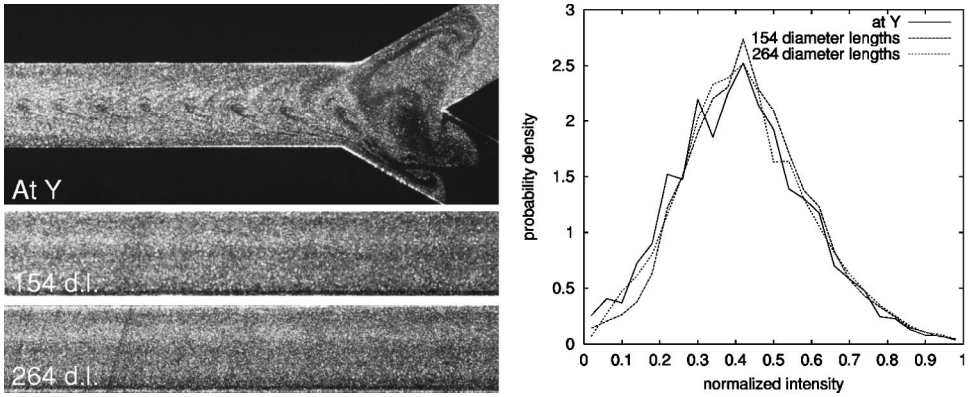

FIG. 13. Histogram plots of experiment 4 with accompanying pictures at different diameter lengths.

$$\bar{x} = \int_0^1 x p(x) dx. \tag{2}$$

To establish a baseline for ''ideal'' mixing, a normalized histogram plot was done on the image of a homogeneous section of seeded fluid, and used to determine a mixing parameter. At the opposite extreme, the mixing parameter for completely unmixed streams is found by taking the first moment of the histogram for a typical image of the peristaltic flow near the Y-connection. The evolution of the mixing parameter for various experiments, as a function of distance from the Y-connection, is plotted in Fig. 14. Clearly, the length of tube required to achieve steady-state conditions is much smaller with the pinch valves than with the peristaltic action alone. The baseline for ideal mixing is at $M_\infty = 0.12$. The mixing parameter for unmixed flow is $M_0 = 0.28$. Using these, the percent fraction of ideal mixing for a given experiment is given by

$$\Delta = 100 \times \frac{M_0 - M}{M_0 - M_\infty}. \tag{3}$$

Table II shows the the steady-state percentage mixing for the peristaltic pump and for different representative experiments.

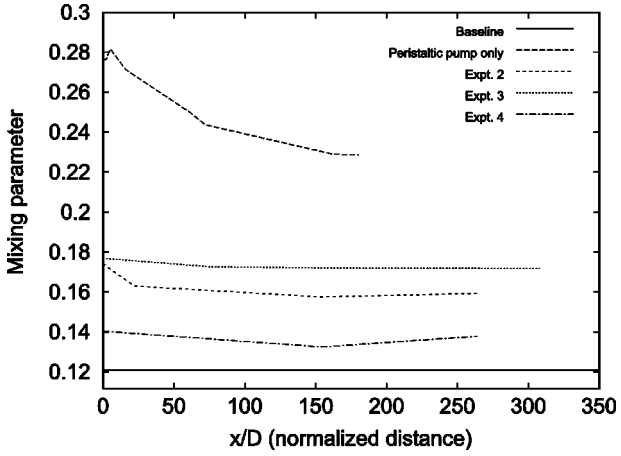

FIG. 14. Plot of mixing parameter as a function of distance past the Y-connection.

It is interesting to note that the mixing in experiment 2 is better than in experiment 3, although the period for experiment 2 is larger than for experiment 3. However, both pulse width and delay are smaller compared to the period in experiment 2. This shows that all timing parameters play a significant role in mixing behavior. The best mixing percentages for experiments 4 and 6 are similar, however, the observed mixing for experiment 6 takes place just after the Y-connection, 3–5 diameter lengths down the tube, whereas the maximum mixing achieved by experiment 4 appears to take longer.

The mixing enhancement in Table II appears to be closely connected to increased length of the mixing interface. The latter can be inferred from the flow images (postprocessed as described above) as follows. For any intensity level, a corresponding intensity isocontour can be plotted. Its length varies with intensity (Fig. 15), however, within a considerable range of intensities (B to C) it remains nearly constant, with the corresponding isocontour largely retaining its appearance. The intensity range within which the boundary between light and dark streams is well-defined decreases with downstream distance because of diffusion, so our analysis of the interfacial properties concentrates on the immediate vicinity of the Y-connection.

For the flow regimes we investigated, the middle of the intensity range between contours ''B'' and ''C'' as illustrated in Fig. 15 corresponds to normalized intensity of 0.35 ± 0.05. This intensity value is selected to define the ''mixing interface'' isocontour in the subsequent analysis. Figure 16 shows the relationship between the steady-state interface length near the Y-connection (ensemble averaged over 12 images) and percentage mixing (Table II). The interface length is normalized by the length of the section visualized (5.3 diameters). There is a striking difference between the

TABLE II. Steady-state percent mixing for different experiments.

Experiment	Best mixing
Peristaltic pump only	31%
Experiment 2	77%
Experiment 3	67%
Experiment 4	93%
Experiment 6	94%

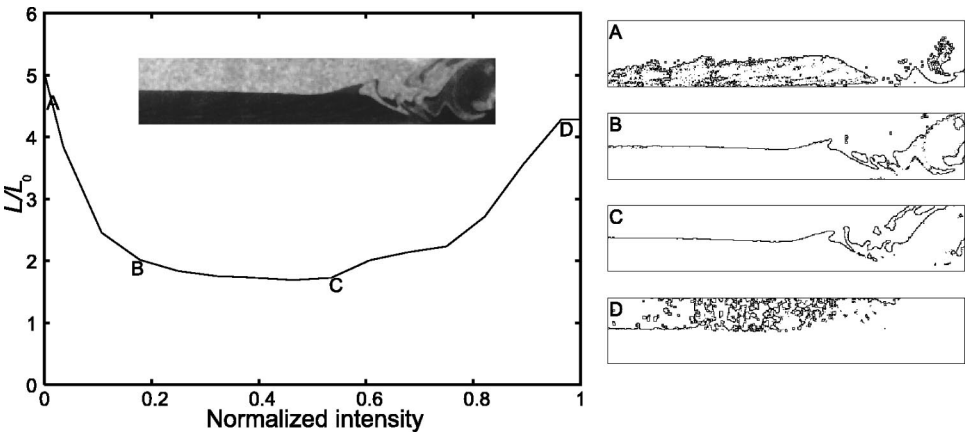

FIG. 15. Lengths of normalized intensity isocontours for the fifth instantaneous image shown in Fig. 9 (experiment 5, dimensionless time 0.451). Letter labels on the graph correspond to isocontours shown on the right.

interface length for the peristaltic-pump flow and the pinch-valve-driven flows. The overall trend the graph shows is for mixing quality to improve with the growth of interface length. However, the definition of the mixing interface illustrated in Fig. 15 fails in image areas with the strongest mixing (experiments 4 and 6), thus leading to less statistically reliable results for these flows.

The enhanced mixing in turbulent flows is strongly linked to complex interface geometry. The connection between fractals and turbulence was first suggested in Ref. [21], and subsequent experiments in turbulent flows [22] demonstrated a range of scales of the mixing interface to have fractal properties. Although our low-Reynolds number mixing flow is distinctly nonturbulent, can enhanced mixing in it be also associated with fractal interface geometry? To answer this question, we estimate the fractal dimension of the mixing interface defined as described above. For the estimate of the Hausdorff dimension of the interface D_H, we employ the box-counting procedure [23]. Figure 17 shows the evolution of the interface fractal dimension for the transient startup flow shown in Fig. 9. Fractal dimension of 1 denotes a linear object, whereas two-dimensional sections of preturbulent and turbulent mixing interfaces are usually characterized by fractal dimensions between 1.3 and 1.4 [24,25]. The evolution of the fractal dimension for our transient flow shows a simple trend: as the interface evolves from nearly linear at early times to the highly distorted steady-state morphology, the fractal dimension increases from unity to about 1.4, the latter value characterizing the steady state.

Figure 18 shows a comparison of some steady-state results for the peristaltic pump-driven flow and flows with the pinch valves. The relationship between the interface fractal dimension and the mixing quality as defined in Table II appears to be monotonic. In a sense, the interface fractal dimension is more strongly related to mixing than the interface length.

If the mean-flow component is absent (Fig. 10), the growth of the mixing-interface length initially follows a trend similar to that reported by Leong and Ottino [11], who observed exponential interface length growth in a low-Reynolds number chaotically mixing cavity flow. They also state that the exponent β in the expression for stretching $A = A_0 \exp(\beta t)$ can be construed as an average Liapunov exponent, positive value of the latter indicating chaotic flow character. Our results presented in Fig. 19 are initially consistent with exponential growth (exponential fit denoted by dashed

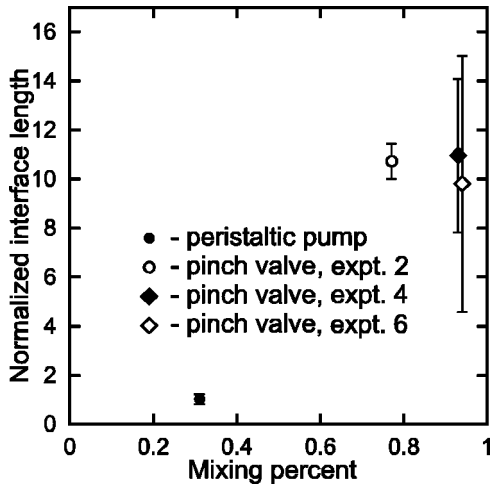

FIG. 16. Normalized ensemble-averaged mixing interface length (vertical axis) versus steady-state mixing percent (horizontal axis). Error bars denote the standard deviation of ensemble-averaged results.

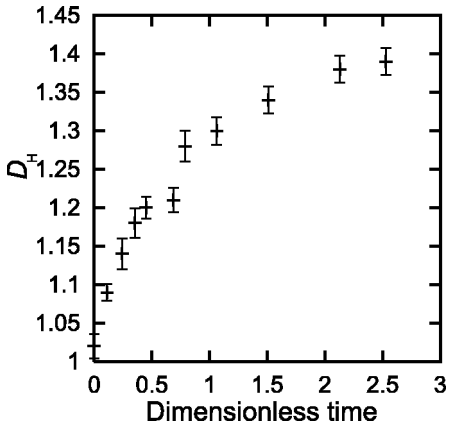

FIG. 17. Box-counting estimate of the fractal dimension D_H of the mixing interface for the transient flow upon startup of the mixer for the parameters of experiment 5 (Fig. 9). Error bars denote the error of the fit used to extract the fractal dimension estimate [23].

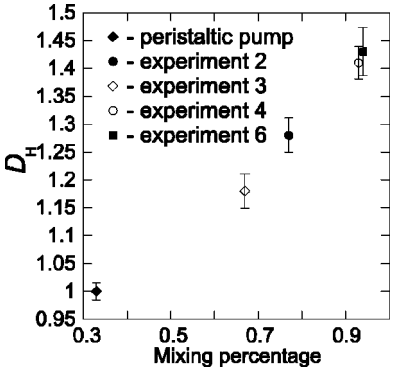

FIG. 18. Steady-state fractal dimension D_H estimate for the peristaltic-pump flow and flows in experiments 2, 3, 4, and 6 versus mixing percent (Table II). Measurements corresponding to specific experiments are labeled in the graph.

line). At late times, the mixing-interface tracing algorithm becomes unreliable—both due to interface striations thinning out beyond the resolution of the camera and due to the interface growing more diffuse. As a consequence of this, the measured mixing-interface length changes its trend of growth, asymptoting to a limit value dictated by the spatial and intensity-level limitations of the acquisition system. Prior to this stage, however, the fit with exponent $\beta=0.407$ describes the dependence of normalized mixing-interface length upon dimensionless time with a standard error of 2.6%. The formula used for curve fitting is $l=\exp(\beta\tau)$, where l and τ are dimensionless interface length and time. Only l values for $\tau<3.9$ were employed for fitting.

Many physical phenomena with a chaotic component (from turbulence to evolution [26]) demonstrate fractal properties. The complex interface geometry of the flow driven by the pinch valves may serve as evidence supporting the notion that the flow is chaotic, however, a rigorous demonstration of chaos would involve time-resolved quantitative analysis including construction of Poincaré sections [13]. The temporal

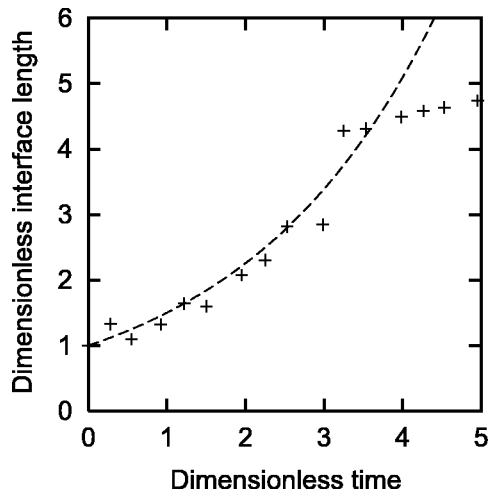

FIG. 19. Normalized mixing interface length as the function of dimensionless time for pinch-valve controlled flow without the mean component (Fig. 10, +). The dashed line denotes exponential fit with exponent 0.407.

resolution of our acquisition system is insufficient for this type of analysis, but we still can quantify disorder in the evolution of the flow to some extent. The boundary conditions applied to the flow are periodic, thus allowing construction of normalized intensity differences

$$I_2^2=\frac{\langle[I(x,y,t)-I(x,y,t+T)]^2\rangle}{\langle I(x,y,t)^2\rangle},$$

where T is the driving period and the $\langle\cdot\rangle$ operator denotes ensemble averaging over several image pairs combined with spatial averaging. The closer the flow to periodic, the lower should the I_2^2 value be. To test this notion, we performed comparison between the peristaltic-pump results and the results from experiment 6, with ensemble averaging over 12 T-separated image pairs and space averaging over the Y-section of the apparatus. The period T in the former case corresponds to the period of the interfacial wave caused by the peristaltic-pump action. In the case of the pinch-valve-driven flow, T is the period of the pinch-valve cycle. The I_2^2 value for peristaltic-pump flow is 0.07 ± 0.01, while for Experiment 2 it is 0.27 ± 0.02, showing a considerable increase in the temporal disorder. It is also of interest that changing the time delay between image pairs from T to $2T$ and $3T$ produces no significant change in the results.

V. CONCLUSION

In this study, a low-Reynolds number mixing flow is driven through a Y-connection by peristaltic pumping. Peristaltic pumps are commonly used in chemical and biological applications because contact of the working fluid with moving parts is eliminated and because of the simplicity of their operation. Flow visualization of two pump-driven mixing streams reveals the unsteadiness of the flow resulting in limited interface distortion, which is amplified by the Poiseuille flow, leading to increased diffusion. Care should be taken to ensure that the pulsations in the incoming streams are in antiphase to maximize the interface distortion. However, mixing solely due to peristaltic pumping is shown to be incomplete, and the oscillatory parameters of the flow are largely predetermined by the choice of the peristaltic pump.

Addition of pinch valves controlled by a timing device to the experimental setup makes it possible to generate a region of disordered flow where large-scale interface distortion occurs. The residence time of fluid in the disordered region is constrained by the mean flow. The limit case of zero mean flow is characterized by the length of the mixing interface between the two streams in the Y-connection growing consistently with exponential law, which suggests that the flow due to the action of the pinch valves is chaotic. Increase in the frequency of operation of the pinch valves leads to increased stretching and folding of the interface, and hence improved mixing. In the cases of improved mixing, the mixing interface appears to acquire fractal properties, while poorly mixing cases are characterized by near trivial interfacial fractal dimension. Within the period of operation of the valves, the interface distortion can be maximized by controlling the length of time each valve is closed, and the delay

between these. Optimization of the latter parameters will be the subject of further research.

If the continuous flow is replaced by samples separated with gas bubbles, the character of the flow within each bubble changes from continuous to recirculating. The timing of the pinch valves that results in optimized mixing should be reexamined for this case. In addition, sensors that detect the presence of a gas bubble may be required to prevent its breakup due to pinch-valve action.

Measurement of the velocity field in the chaotic region by means of particle image velocimetry would allow the analysis of mixing in terms of the formation and motion of coherent structures, as suggested by Leong and Ottino [11]. This would provide a more thorough mathematical understanding of the mixing processes seen to occur in this experiment.

This work could have direct application in high throughput flow cytometry and other areas where continuous mixing of reagents at low Re is needed (for example, food, chemical, printing, biodetection) may also benefit. Because the mixer is effective at low Re, it is particularly suited to microscale applications. In applications where particle-laden fluids are transported, moving or stationary obstacles in the flow may be undesirable. These applications are most likely to benefit from low-Re mixing enhancement technique described in this work.

ACKNOWLEDGMENT

This work was supported by NIH Grant No. GM60799/EB00264.

[1] F. Kuckuck, B. Edwards, and L. Sklar, Cytometry **44**, 83 (2001).
[2] B. Edwards, F. Kuckuck, E. Prossnitz, J. Ransom, and L. Sklar, J. Biomol. Screening **6**, 83 (2001).
[3] R. Chella and J. Viñals, Phys. Rev. E **53**, 3832 (1996).
[4] J. Ottino, S. Jana, and V. Chakravarthy, Phys. Fluids **6**, 685 (1994).
[5] V.S. Chakravarthy and J.M. Ottino, Chem. Eng. Sci. **519**, 3613 (1995).
[6] M. Liu, F. Muzzio, and R. Peskin, in *Chaos Applied to Fluid Mixing*, edited by H. Aref and M. El Naschie (Elsevier Sciences, Amsterdam, 1995), pp. 125–149.
[7] J.M. Ottino, Sci. Am. **260**(1), 56 (1989).
[8] P. Swanson and J. Ottino, J. Fluid Mech. **213**, 227 (1990).
[9] A. Souvaliotis, S.C. Jana, and J.M. Ottino, AIChE J. **41**, 1605 (1995).
[10] S.C. Jana, G. Metcalfe, and J.M. Ottino, J. Fluid Mech. **269**, 199 (1994).
[11] C. Leong and J. Ottino, J. Fluid Mech. **209**, 463 (1989).
[12] A. Strook, S. Dertinger, A. Ajdari, I. Mezic, H. Stone, and G. Whitesides, Science **295**, 647 (2002).
[13] D. Khakhar, J. Franjione, and J. Ottino, Chem. Eng. Sci. **42**, 2909 (1987).
[14] C. Amon, A. Guzman, and B. Morel, Phys. Fluids **8**, 1192 (1996).
[15] K. Selverov and H. Stone, Phys. Fluids **13**, 1837 (2001).
[16] C.A. Taylor, T.J.R. Hughes, and C.K. Zarins, Comput. Methods Appl. Mech. Eng. **158**, 155 (1997).
[17] C.A. Taylor, T.J.R. Hughes, and C.K. Zarins, Ann. Biomed. Eng. **26**, 975 (1998).
[18] C.A. Taylor, T.J.R. Hughes, and C.K. Zarins, J. Vasc. Surg. **29**, 1077 (1999).
[19] D.N. Ku, Annu. Rev. Fluid Mech. **29**, 399 (1997).
[20] W.C. Jackson, F. Kuckuck, B.S. Edwards, A.A. Mammoli, C.M. Gallegos, G.P. Lopez, T. Buranda, and L.A. Sklar, Cytometry **47**, 183 (2002).
[21] B. Mandelbrot, *The Fractal Geometry of Nature* (Freeman, New York, 1982).
[22] K.R. Sreenivasan and C. Meneveau, J. Fluid Mech. **173**, 357 (1986).
[23] J. Theiler, J. Opt. Soc. Am. A **7**, 1055 (1990).
[24] P. Flohr and D. Olivari, Physica D **76**, 278 (1994).
[25] P. Vorobieff, P.M. Rightley, and R.F. Benjamin, Physica D **133**, 469 (1999).
[26] D.M. Green, Trends Ecol. Evol. **6**, 333 (1991).